Modulation Linearity Characterization of Si Ring Modulators

Youngkwan Jo, *Student Member, IEEE*, Christian Mai, Stefan Lischke, *Student Member, IEEE*, Lars Zimmermann, *Senior Member, IEEE*, and Woo-Young Choi, *Member, IEEE*

***Abstract*—Modulation linearity of Si ring modulators (RMs) is investigated through the numerical simulation based on the coupled-mode theory and experimental verification. Numerical values of the key parameters needed for the simulation are experimentally extracted. Simulation and measurement results agree well. With these, the influence of input optical wavelength and power on the Si RM linearity are characterized.**

***Index Terms*—Microwave photonics, modulation linearity, Si ring modulator.**

I. Introduction

PERFORMANCE of microwave photonics (MWP) systems are often strongly influenced by the linearity of optical modulators that convert microwave signals into the optical domain. In particular, the spurious-free dynamic range (SFDR) of the employed optical modulator is the key parameter that determines the performances of such MWP systems as radio-over-fiber (RoF) transmission links [1]–[3], MWP frequency converters [4]–[6], optical beamforming [7], photonic analog-to-digital converters (ADCs) [8] and microwave photonic filters [9], [10]. In recent years, the possibility of achieving MWP functions in a single integrated platform based on Si Photonics is attracting a great amount of research interests [11] and, consequently, the modulation linearity of Si modulators has become an important research topic. In addition, realization of various non-linear MWP or photonics signal-processing devices based on Si such as frequency converters [4]–[6] and optical comb generators [12], [13] requires precise knowledge on linear and nonlinear characteristics of Si modulators. The modulation linearity of the Si Mach-Zehnder modulator (MZM) has been extensively characterized with Taylor series expansion of the transfer function [14], [15] and can be improved with various techniques such as push-pull electrical driving and the differential detection scheme [16] as well as the use of dual-parallel or dual-series MZMs [17].

However, there are only limited published reports on the linearity characteristics of the Si ring modulator (RM), which with the advantages of small footprint, high energy efficiency, and large modulation bandwidth, is the key building block for many high-performance Si photonic systems [18], [19]. In [20], the transfer function of the Si RM is modeled with a Lorentzian function and, with it, the source of nonlinearity is investigated, but detailed linearity characteristics such as the SFDR dependence on the input wavelength or optical power is not provided. In [21], the Si RM is modeled with both the coupled-mode theory (CMT) and the round-trip theory, and the carrier-to-distortion ratio (CDR), SFDR of RM and fiber data transmissions are determined. However, the accuracy of the model is not verified with experimental results. In [22], the Si RM is linearized with the DC Kerr effect in the p-i-n phase shifter and the influence of the bias voltage and the input optical wavelength on the performance is investigated. However, with Taylor series expansion of the Si RM transfer function, very complex analytic expressions are needed for determining distorted signals, which may reduce its applicability to a wider range of Si RM applications. In [23], the Si RM SFDR is improved by reducing the Q factor and selecting the optimum input wavelength, but the difference between analytic calculation and measurement results is not fully explained. Furthermore, none of the previous reports considered the influence of self-heating, which greatly affects the Si RM performance [24], [25].

In this paper, we determine how Si RM linearity characteristics change depending on input wavelength (λ_{in}) and power (P_{in}). For this, numerical analyses based on the CMT are performed, and the results are verified with experimental measurement. These results allow one to select the optimal Si RM λ_{in} and P_{in} for the desired target linear or nonlinear applications. This paper is organized as follows. In Section II, the CMT model for the Si RM is briefly reviewed, the process of extracting model parameters from the measurement is explained, and our method of numerical simulation of Si RM linearity is explained. In Section III, the accuracy of the numerical simulation is verified with the measurement results. Section IV concludes the paper.

Manuscript received March 20, 2021; revised June 17, 2021; accepted June 25, 2021. Date of publication June 29, 2021; date of current version December 16, 2021. This work was supported by the National Research Foundation of Korea (NRF) grant funded by the Korea government (MSIT) under Grant NRF-2020R1A2C2015089. *(Corresponding author: Woo-Young Choi.)*

Youngkwan Jo and Woo-Young Choi are with High-Speed Circuits and Systems Laboratory, Department of Electrical and Electronic Engineering, Yonsei University, Seoul 03722, South Korea (e-mail: kwan0122@yonsei.ac.kr; wchoi@yonsei.ac.kr).

Christian Mai and Stefan Lischke are with the IHP—Leibniz Institute für Innovative Mikroelektronik, 15236 Frankfurt, Germany (e-mail: cmai@ihpmicroelectronics.com; lischke@ihp-microelectronics.com).

Lars Zimmermann is with the IHP—Leibniz Institute für Innovative Mikroelektronik, 15236 Frankfurt, Germany and also with Technische Universitaet Berlin, 10587 Berlin, Germany (e-mail: lzimmermann@ihp-microelectronics.com).

Color versions of one or more figures in this article are available at https://doi.org/10.1109/JLT.2021.3093463.

Digital Object Identifier 10.1109/JLT.2021.3093463

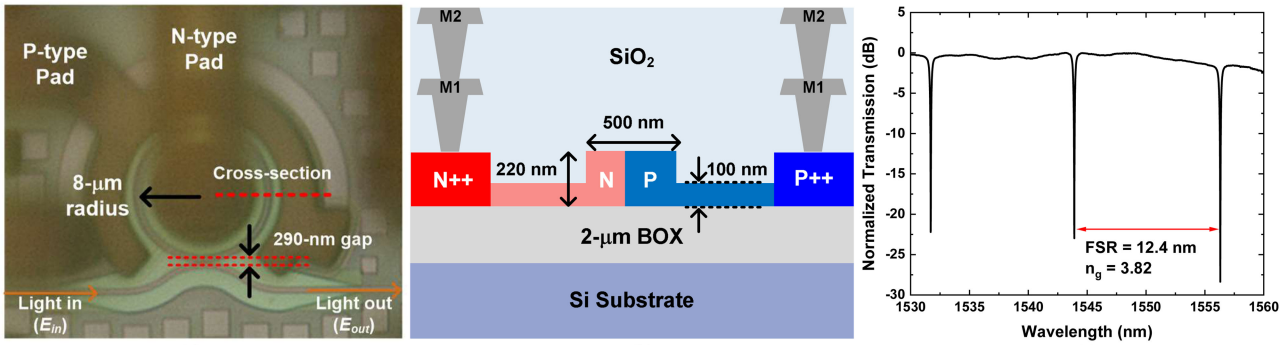

(a) (b) (c)

Fig. 1. (a) Microphotograph of fabricated chip, (b) cross-section diagram and (c) measured broadband transmission spectrum of Si RM.

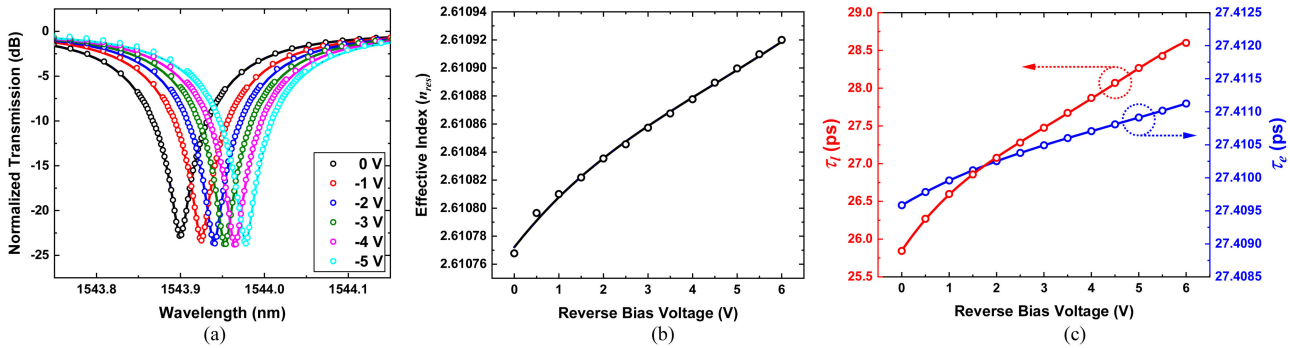

(a) (b) (c)

Fig. 2. (a) Measured transmission spectra of near λ_{res}, (b) extracted effective refractive index (n_{res}) and (c) extracted τ_l, τ_e.

II. Si RM Linearity Analysis Based on CMT Model

Fig. 1(a) shows a micro-photograph of a fabricated depletion-type Si RM used for our investigation, which is fabricated by IHP's Si Photonics technology. It has 8-μm ring radius, 290-nm gap between ring and bus waveguides, both of which are 500-nm wide rib waveguides having 220-nm rib and 100-nm slab thickness as shown in Fig. 1(b). In the lateral PN junction, the nominal peak carrier densities are 7×10^{17}/cm^3 for the p-region and 3×10^{18}/cm^3 for the n-region. Fig. 1(c) shows the measured transmission spectrum of Si RM around 1.55μm, which has the FSR of 12.4 nm with group refractive index of 3.82.

Using the coupled-mode theory, the dynamic behavior of the RM in the time domain can be described as [27]

$$\frac{d}{dt}a(t) = \left(j\omega_{res} - \frac{1}{\tau}\right)a(t) - j\sqrt{\frac{2}{\tau_e}}E_{in}(t), \quad (1)$$

$$E_{out}(t) = E_{in}(t) - j\sqrt{\frac{2}{\tau_e}}a(t), \quad (2)$$

where $a(t)$ represents the energy amplitude inside the ring and τ is its decay time constant. τ has two contributions, τ_l and τ_e, where τ_l is the decay time constant due to round-trip loss inside the ring waveguide and τ_e due to the coupling between the ring and bus waveguides. Their relationship is given as $1/\tau = 1/\tau_l + 1/\tau_e$. ω_{res}, the resonance angular frequency, is given as $2\pi mc/n_{res}L$, where m is an integer, c is the speed of light in vacuum, L is the ring circumference, and n_{res} is the ring waveguide effective index at ω_{res}. E_{in} and E_{out} represent the input and output E-field of the RM, respectively. Using above equations, the RM transient modulation characteristics can be numerically determined when the RM is modulated with RF signals, which results in changes of n_{res}, τ_l and τ_e. The numerical values for these model parameters at different bias voltages can be extracted by the steady-state transmission characteristics derived from (1) and (2) given as

$$T = \left|\frac{E_{out}}{E_{in}}\right|^2 = \left|\frac{j(\omega - \omega_{res}) + \frac{1}{\tau_l} - \frac{1}{\tau_e}}{j(\omega - \omega_{res}) + \frac{1}{\tau_l} + \frac{1}{\tau_e}}\right|^2 \quad (3)$$

to the measured transmission spectra at different bias voltages.

Fig. 2(a) shows the measured and fitted transmission spectra at different bias voltages. The extracted parameter values that provide the best fitting are shown in Fig. 2(b) for n_{res} and in Fig. 2(c) for τ_e, τ_l. As can be seen, all these parameters show nonlinear dependence on the bias voltage, which in turn affects Si RM linearity. For the measurement results shown in Fig. 2(a) as well as other measurement results provided in this paper, the Si RM is placed on the probing stage whose temperature is maintained at 25°C by a temperature controller.

In addition to these three CMT model parameters, the Si RM electrical characteristics must be considered for accurate analysis. Fig. 3(a) shows the electrical equivalent circuit for the Si RM, which consists of parasitic components due to pads and metal interconnect [26], series resistance (R_s) and voltage-dependent junction capacitance (C_j) of the PN diode within the Si RM. Their numerical values can be determined by fitting

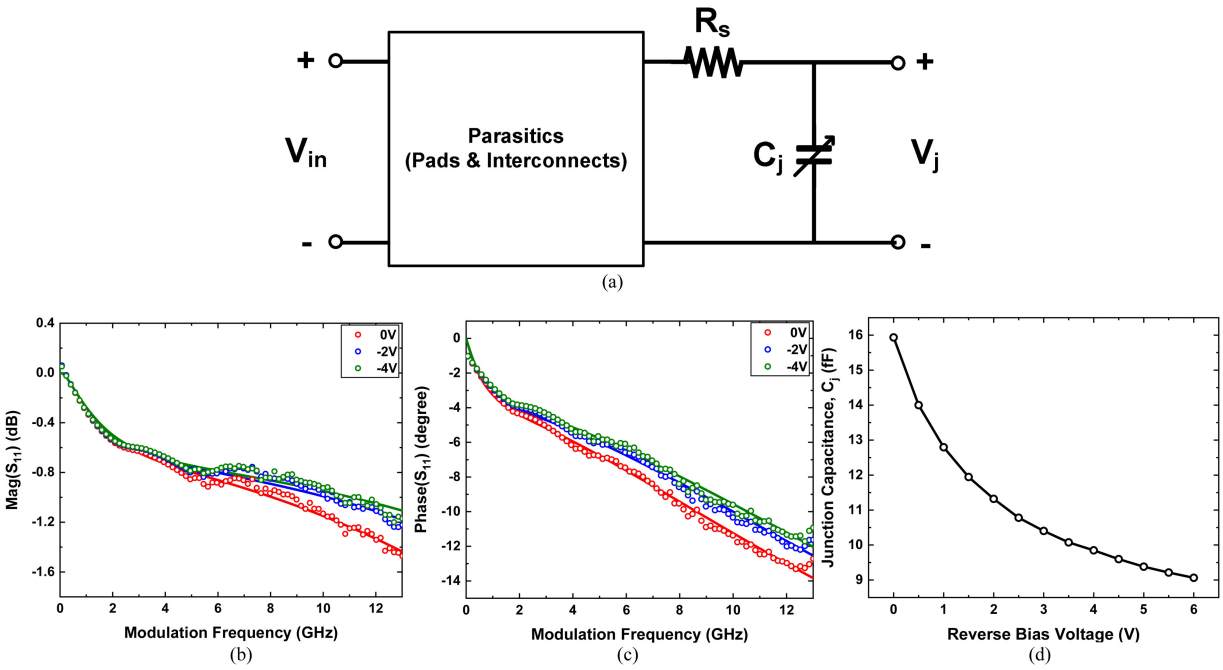

Fig. 3. (a) Block diagram for electrical equivalent circuit of RMs. (b) Magnitude and (c) phase of measured S_{11} for different reverse bias voltages. (d) Extracted junction capacitance (C_j).

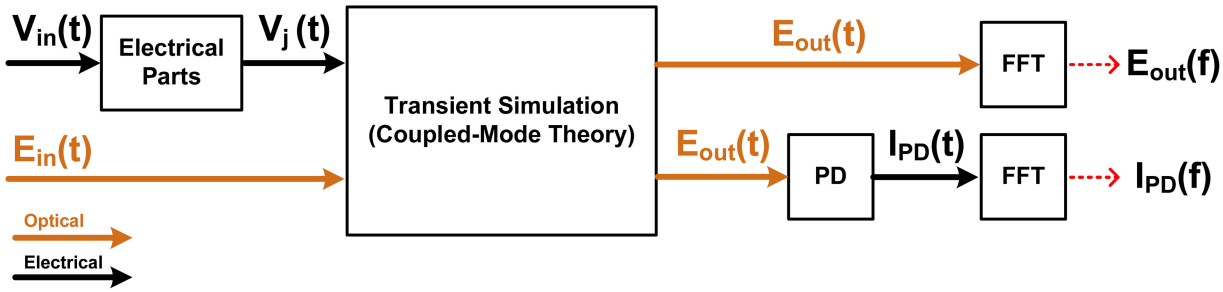

Fig. 4. Block diagram for characterization of RM for modulation linearity analysis.

the simulated reflection coefficients (S_{11}) to the measurement results. Fig. 3(b) and (c) respectively show the measured and the fitted magnitude and phase frequency responses for Si RM S_{11} at different bias voltages. For best fitting, the value of R_s in the equivalent circuit is determined to be 240 Ω independent of bias voltages. The dependence of extracted C_j values on the bias voltage is shown in Fig. 3(d). This nonlinear capacitor can also influence Si RM linearity.

Fig. 4 schematically shows how the Si RM linearity is numerically analyzed in this investigation. When RF signals, $V_{in}(t)$, are applied to a Si RM, the voltage applied to the PN junction of Si RM, $V_j(t)$, at a given time is first determined using the nonlinear filter response of the electrical equivalent circuit shown in Fig. 3(a) with the extracted circuit parameter values. For handling the nonlinear junction capacitor, a piecewise-linear voltage-controlled capacitor available in Cadence Virtuoso 6.1.6 is used. Then, the time-domain response of $E_{out}(t)$ is determined by numerically solving (1) and (2) using the voltage-dependent τ_e, τ_l and n_{res} values. From the magnitude of the Fourier-transform of $E_{out}(t)$, the optical spectrum of the Si RM can be determined. An example for the resulting optical spectrum is shown in Fig. 5(a) when the Si RM biased at -2 V is modulated with 10-GHz, 2-$V_{\text{peak-to-peak}}$ (10-dBm) RF signals. The spectrum shows several sidebands separated by multiples of 10-GHz (∼80 pm) from λ_{in} of 1543.9 nm. For this simulation, λ_{in} is assumed to be 40 pm smaller than the Si RM resonance wavelength (λ_{res}) at the bias voltage of -2 V as shown in the inset of Fig. 5(a). The background level in Fig. 5(a) is due to the numerical truncation error during Fourier transform of $E_{out}(t)$. Furthermore, by taking the Fourier-transform of $|E_{out}(t)|^2$, the RF spectrum of the photodetected Si RM output signals can be obtained. Fig. 5(b) shows the resulting RF spectrum when the Si RM biased at -2 V is modulated by two-tone RF signals of 9.9-GHz and 10.1-GHz, both of which have 10-dBm RF power. For this, λ_{in} of 1543.9 nm is also assumed. In the figure, the third-order intermodulation (IMD3) signals are clearly visible that are separated by 200MHz from each of the fundamental

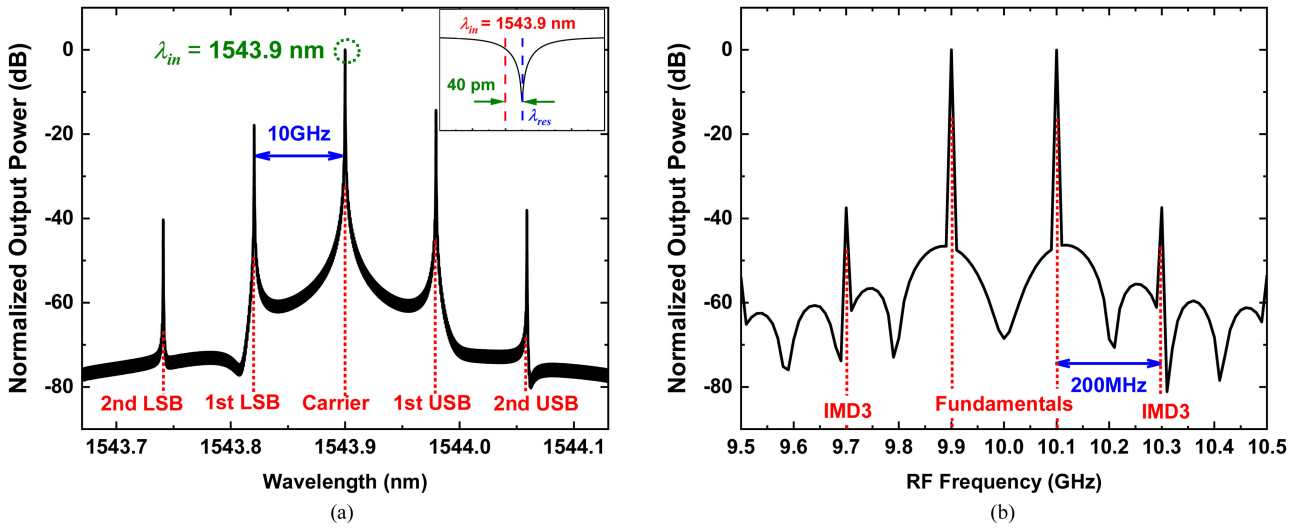

Fig. 5. (a) Simulated optical spectrum when RM is modulated with one-tone, 10-GHz RF signal and (b) simulated electrical spectrum when RM is modulated with two-tone, 9.9-GHz and 10.1-GHz RF signals. The RM is biased at −2 V, and the RF signal has 2-$V_{\text{peak-to-peak}}$. λ_{in} for both cases is 1543.9 nm, and the simulation is based on the extracted parameters in Fig. 2 and 3.

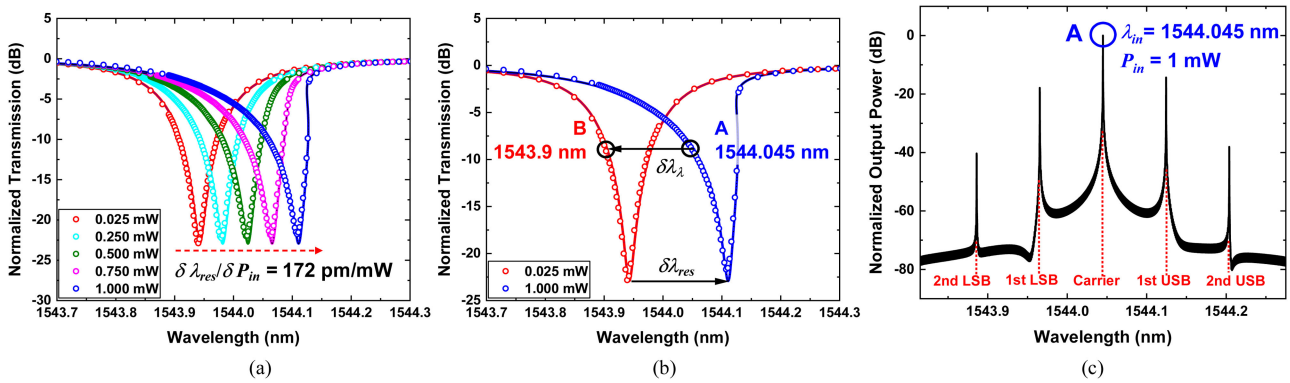

Fig. 6. (a) Measured transmission spectra of RM for 0.025-mW, 0.250-mW, 0.500-mW, 0.750-mW, and 1.000-mW of P_{in} and extracted $\delta\lambda_{res}/\delta P_{in}$ value. (b) Measured transmission spectra of RM for 0.025-mW and 1.000-mW of P_{in}. (c) the optical spectra when the RM is modulated with 10-GHz, 2-$V_{\text{peak-to-peak}}$ RF signal for the Point A in Fig. 6(b).

tone. These IMD3 signals are due to the Si RM nonlinearity. By repeating this two-tone RF modulation analysis for different RF modulation powers, the Si RM SFDR can be determined.

In the Si RM, P_{in} changes the transmission spectrum due to self-heating [24]. Fig. 6(a) shows the normalized measured transmission spectra for five different P_{in} values. As shown in the figure, λ_{res} red-shifts linearly as P_{in} increases with $\delta\lambda_{res}/\delta P_{in}$ of about 172 pm/mW, which corresponds to 2.91 x 10^{-4}/mW of $\delta n_{res}/\delta P_{in}$. However, $\delta n_{res}/\delta P_{in}$ has two components, one due to self-heating and the other due to dispersion. With the known value of -1.85 x 10^{-4} /mW for dispersion in Si around 1.5 μm [28], $\delta n_{res}/\delta P_{in}$ purely due to self-heating can be determined to be 4.76 x 10^{-4} /mW. With the coefficients for the Kerr effect and two-photon absorption at 1.55 μm in Si of 3∼6 x 10^{-18} m^2/W [29], [30] and 0.7 cm/GW [31], respectively, these two effects can be ignored with the range of P_{in} used in this investigation.

Since self-heating only influences the static characteristics of the Si RM and not the dynamic characteristics, the dynamic

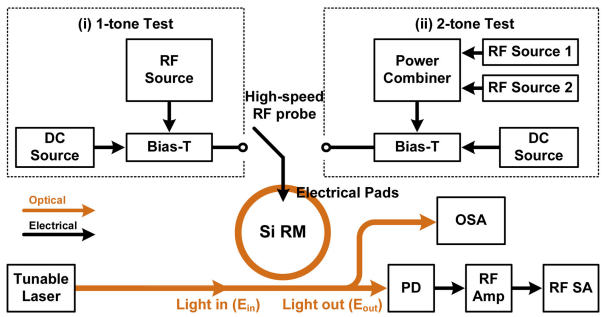

Fig. 7. Measurement setup for verification of model.

analysis for the Si RM under self-heating at a given λ_{in} can be performed by assuming λ_{in} is shifted to a certain amount to the left and using model parameters at this low P_{in} without self-heating [25]. For an example, when $\lambda_{in} = 1544.045$ nm and $P_{in} = 1$ mW corresponding to Point A in Fig. 6(b), the linearity analysis can be performed assuming Point A is shifted to Point

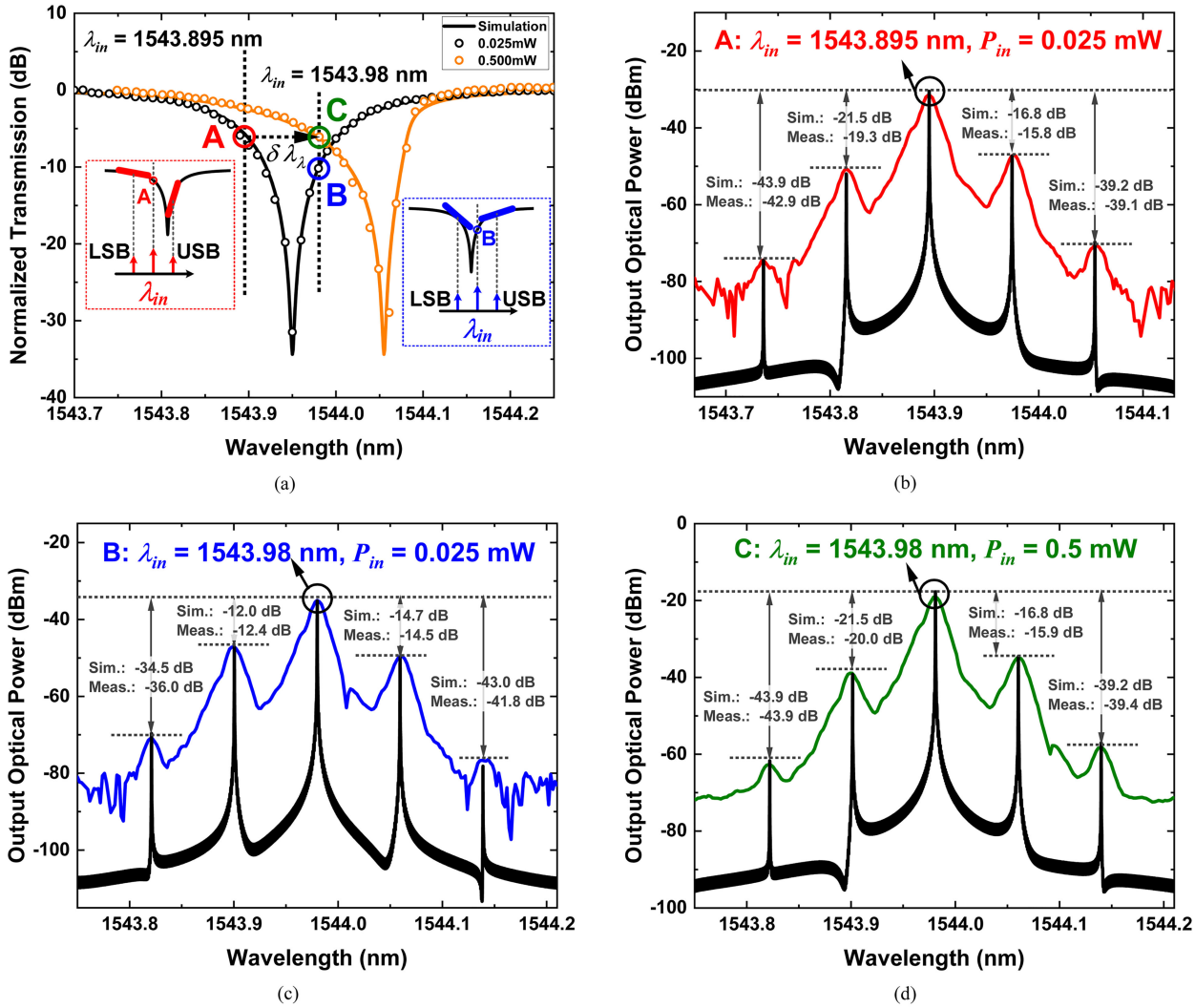

Fig. 8. (a) Measured normalized transmission spectra of RM with 0.025 mW and 0.5 mW of P_{in}. Measured and simulated optical spectra where the RM is modulated with 10-GHz, 2-$V_{\text{peak-to-peak}}$ RF signal for the point A, B and C in (a) are shown in (b), (c) and (d), respectively. Each graph shows the simulated and measured ratio of carrier to sideband signals.

B in the transmission spectrum for low P_{in} without self-heating. The exact amount of wavelength shifted needed ($\delta\lambda_\lambda$) is given below [24], but basically two points (A and B) should have the same amount of normalized transmission.

$$\delta\lambda_\lambda = \delta n_{res}\frac{L}{m}\left|\frac{\frac{1}{\tau}}{j(\omega-\omega_{res})+\frac{1}{\tau}}\right|^2, \tag{4}$$

where δn_{res} presents the difference in the effective index at λ_{res} for high and low P_{in}'s, and ω, ω_{res}, τ are values for low P_{in}. Fig. 6(c) shows the optical spectrum for Point A obtained with this technique. The result is essentially the same as the optical spectrum shown in Fig. 5(a) with the exception of the wavelength values that are larger by the amount of 145 pm, determined by (4).

III. Si RM Linearity Measurement

Fig. 7 shows the measurement setup used for Si RM modulation linearity characterization. For the one-tone measurement, 10-GHz, 10-dBm RF signals are supplied to the device through RF probes with the DC-bias voltage of -2 V provided through a bias-T. The bias voltage of -2 V is used because with a smaller bias voltage the PN junction in the RM can reach the forward bias region resulting in clipping when RF modulated, and with a larger bias voltage there is a danger of junction breakdown for the RM when RF modulated. In addition, the Si RM SFDR does not strongly depend on the bias voltage [22] as long as the PN junction in the RM does not reach the forward bias region or breakdown when RF modulated. In the case of the two-tone test, two RF signals having 9.9-GHz and 10.1-GHz both having 10-dBm are combined with a power combiner and supplied to the device. For optical I/O, grating couplers are used. An optical spectrum analyzer is used for measuring optical spectra, and a photodetector, an RF amplifier, and an RF spectrum analyzer are used for measuring RF spectra.

Fig. 8(a) shows how the measured and the simulated optical carrier power changes when λ_{in} changes. For this, the Si RM is modulated with 10-GHz, 10-dBm RF signals and two different P_{in} values of 0.025 mW and 0.5 mW are used. These

results are essentially the same as the transmission spectra for the corresponding P_{in} shown in Fig. 6(a). Fig. 8(b), (c) and (d) show the measured and simulated optical spectra for the conditions represented by Point A ($\lambda_{in} = 1543.895$ nm, $P_{in} = 0.025$ mW), B ($\lambda_{in} = 1543.98$ nm, $P_{in} = 0.025$ mW) and C ($\lambda_{in} = 1543.98$ nm, $P_{in} = 0.5$ mW) in Fig. 8(a), respectively. For all of these cases, the measured ratios of the sideband peak powers to the carrier powers agree well with the simulated values as shown in the figures, indicating the accuracy of our simulation regardless of λ_{in} and P_{in}.

When λ_{in} is smaller than λ_{res}, which is the case for Point A, the lower sidebands have smaller peak values than the upper sidebands as can be seen in Fig. 8(b) and (d). This is because the magnitude of the transmission spectrum slope for λ_{in} lower than λ_{res} is smaller than that for λ_{in} higher than λ_{res} as graphically shown in the insets of Fig. 8(a). In contrast, at Point B, the opposite is the case as can be seen in Fig. 8(c).

Fig. 9(a) and (b) show the measured and the simulated peak powers for the optical carrier and other sidebands when λ_{in} changes for P_{in} of 0.025 mW and P_{in} is 0.5 mW. Clearly, when using the Si RM as a linear modulator, a great care is required in selecting λ_{in} and P_{in} so that the desired peak values, for example for the 1st sidebands, can be enlarged as much as possible and undesired peak values such as the 2nd sidebands can be suppressed as much as possible.

For the RF spectrum measurement, a larger P_{in} is needed so that a sufficient amount of the photocurrents is produced. In addition, an RF amplifier is needed to make the PD output detectable. The PD used in the measurement has a responsivity of 0.63 A/W and the RF amplifier has 1-dB gain compression power larger than 10-dBm. We carefully selected P_{in} and the RF amplifier gain so that the PD and the RF amplifier by themselves do not suffer from any nonlinear effect. Fig. 10(a) shows the measured RF spectrum when the Si RM is modulated with 9.9-GHz and 10.1-GHz, 1.25-$V_{\text{peak-to-peak}}$ (6-dBm) RF signals with P_{in} of 0.5 mW and λ_{in} of 1544.09 nm which is 30 pm larger than λ_{res}. The measured ratio of the fundamental to the IMD3 is 58.51 dB, which is close to the simulated value of 57.36 dB.

For SFDR determination, the fundamental and the IMD3 signals are measured with increasing the RF power for two-tone signals. The measured as well as the simulated results are shown in Fig. 10(b). For this, the same values of P_{in} and λ_{in} as in Fig. 10(a) are used. For the noise floor determination [32], the relative intensity noise (RIN) of about -140 dB/Hz is used for the tunable laser. The load impedances for the PD and the RF amp are both 50 ohms, and bandwidth for the noise calculation is assumed as 1 Hz. For link calculation needed for the shot noise and relative intensity noise (RIN), the insertion loss of the Si RM that depends on λ_{in} is considered as well as the insertion loss due to the grating couplers. Tunable laser source is controlled to have a 4.2-dBm output power to deliver 0.5 mW of P_{in} for the RM, considering the insertion loss due to two grating couplers, 14.4 dB. The insertion loss of RM at the same values of P_{in} and λ_{in} as in Fig. 10(a) is 1.9 dB which leads to -12.1 dBm input power for the photodetector, resulting in

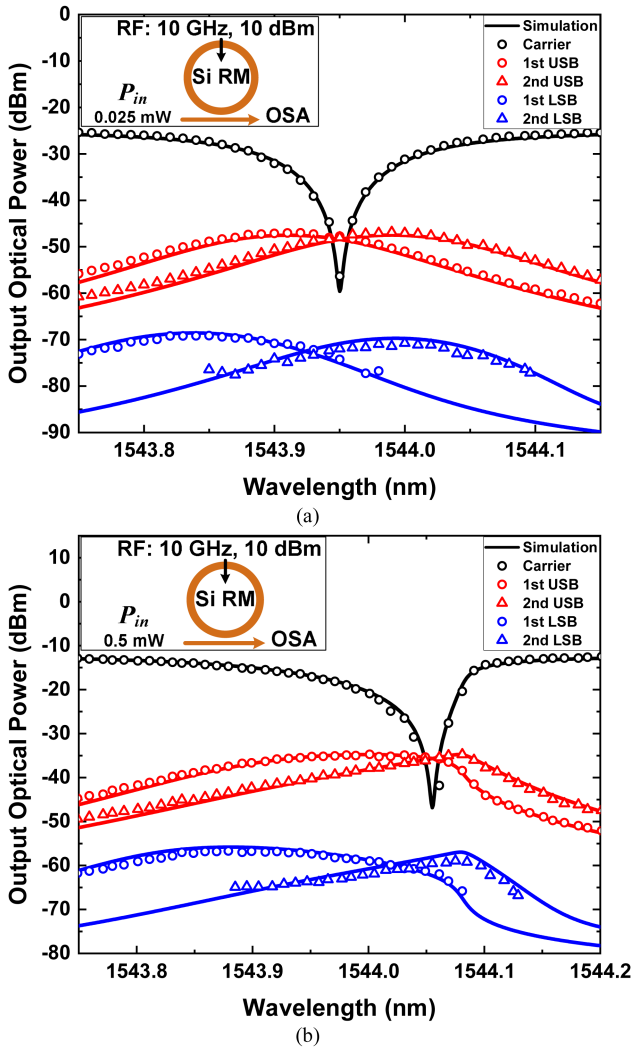

Fig. 9. The measured and simulated peak optical power of each tone corresponding to λ_{in} for (a) 0.025 mW of P_{in} and (b) 0.5 mW of P_{in}, where RM is modulated with 10-GHz, 2-$V_{\text{peak-to-peak}}$ RF signal.

0.039 mA of photocurrent. At this point, the shot and RIN noise are -182.11 dBm and -181.34 dBm, which is significantly smaller than the thermal noise of -173.85 dBm. Then, the noise floor is determined as -172.63 dBm, which results in SFDR of 95.39 dB·$Hz^{2/3}$. For the cases of λ_{in} nearer to the λ_{res}, the insertion loss of RM becomes even larger so that the total noise is dominated by the thermal noise [22], [33]. Fig. 10(c) shows the measured and the simulated Si RM SFDR's as function of λ_{in} at three different P_{in} values. Since P_{in} has a negligible influence on the noise floor, the SFDR become larger as P_{in} increases simply because output signal power of Si RM increases, showing asymmetric shift of SFDR curve for large value of P_{in}. Clearly, a careful selection of λ_{in} and P_{in} is needed for a given Si RM so that its SFDR can be maximized for linear applications. Once again, the simulated results agree well with the measurement results.

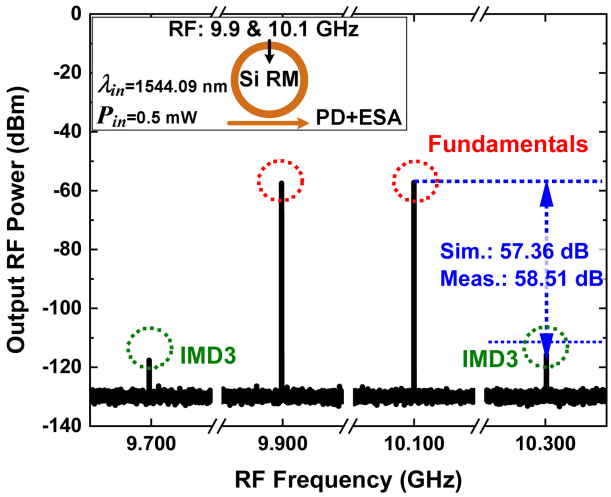

(a)

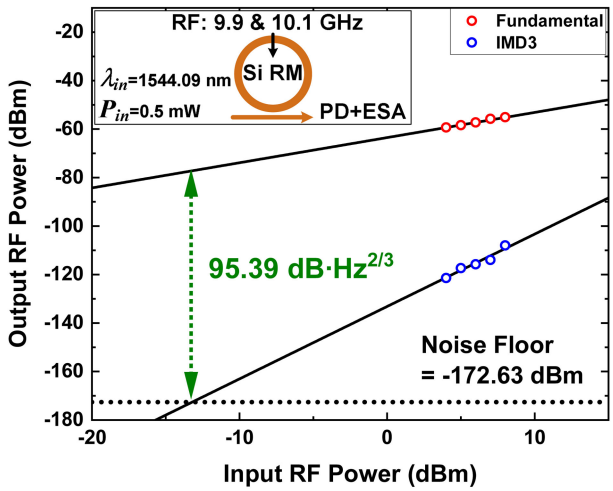

(b)

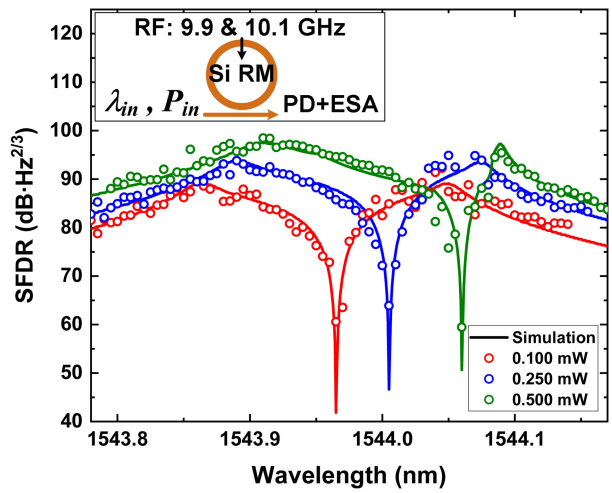

(c)

Fig. 10. (a) Measured RF spectrum for 0.5 mW of P_{in} where RM is modulated with 9.9-GHz, 10.1-GHz and 1.25-$V_{peak\text{-}to\text{-}peak}$ RF signals at 1544.09 nm of λ_{in}. (b) Measured power of fundamental and IMD3 signals, SFDR value at 1544.09 nm. (c) Measured SFDR of RM with different P_{in} of RM. 0.100-mW, 0.250-mW and 0.500-mW of P_{in} for red-, blue- and green-line, respectively.

IV. Conclusion

It is demonstrated that the Si RM linearity can be very accurately modeled by numerically solving the CMT transient model of the Si RM and performing necessary Fourier transforms if the required model parameter values are carefully extracted. When a Si RM is modulated with RF signals, our technique can provide accurate results for optical spectra, RF spectra, as well as SFDRs, as verified with the measurement results for various values. With this technique, the optimal condition of the Si RM λ_{in} and P_{in} can be determined for the desired linear or nonlinear applications.

References

[1] T. Kurniawan, A. Nirmalathas, C. Lim, D. Novak, and R. Waterhouse, "Performance analysis of optimized millimeter-wave fiber radio links," *IEEE Trans. Microw. Theory Techn.*, vol. 54, no. 2, pp. 921–928, Feb. 2006, doi: 10.1109/TMTT.2005.863047.

[2] C. Lim, A. Nirmalathas, K. Lee, D. Novak, and R. Waterhouse, "Intermodulation distortion improvement for fiber–radio applications incorporating OSSB+C modulation in an optical integrated-access environment," *J. Lightw. Technol.*, vol. 25, no. 6, pp. 1602–1612, Jun. 2007, doi: 10.1109/JLT.2007.896814.

[3] D. Novak *et al.*, "Radio-over-fiber technologies for emerging wireless systems," *IEEE J. Quantum Electron.*, vol. 52, no. 1, pp. 1–11, Jan. 2016, Art. no. 0600311, doi: 10.1109/JQE.2015.2504107.

[4] C. G. Bottenfield and S. E. Ralph, "High-performance fully integrated silicon photonic microwave mixer subsystems," *J. Lightw. Technol.*, vol. 38, no. 19, pp. 5536–5545, Oct. 2020.

[5] A. M. Gutiérrez *et al.*, "Silicon slow-light-based photonic mixer for microwave-frequency conversion applications," *Opt. Lett.*, vol. 37, pp. 1721–1723, 2012.

[6] Y. Pan *et al.*, "Adaptive linearized microwave downconversion utilizing a single dual-electrode Mach–Zehnder modulator," *Opt. Lett.*, vol. 40, pp. 2649–2652, 2015.

[7] C. Vagionas *et al.*, "Linearity measurements on a 5G mmWave fiber wireless IFoF fronthaul link with analog RF beamforming and 120° degrees steering," *IEEE Commun. Lett.*, vol. 24, no. 12, pp. 2839–2843, Dec. 2020, doi: 10.1109/LCOMM.2020.3019733.

[8] G. C. Valley, "Photonic analog-to-digital converters," *Opt. Exp.*, vol. 15, pp. 1955–1982, 2007.

[9] L. Huang *et al.*, "A linearized tunable single bandpass microwave photonic filter," *IEEE Microw. Wireless Compon. Lett.*, vol. 26, no. 11, pp. 963–965, Nov. 2016, doi: 10.1109/LMWC.2016.2615031.

[10] X. Han, E. Xu, and J. Yao, "Tunable single bandpass microwave photonic filter with an improved dynamic range," *IEEE Photon. Technol. Lett.*, vol. 28, no. 1, pp. 11–14, Jan. 2016, doi: 10.1109/LPT.2015.2478856.

[11] D. Marpaung *et al.*, "Integrated microwave photonics." *Laser Photon. Rev.*, vol. 7, no. 4, pp. 506–538, 2013.

[12] I. Demirtzioglou *et al.*, "Frequency comb generation in a silicon ring resonator modulator," *Opt. Exp.*, vol. 26, pp. 790–796, 2018.

[13] Y. Xu, J. Lin, R. Dubé-Demers, S. LaRochelle, L. Rusch, and W. Shi, "Integrated flexible-grid WDM transmitter using an optical frequency comb in microring modulators," *Opt. Lett.*, vol. 43, pp. 1554–1557, 2018.

[14] A. M. Gutierrez *et al.*, "Analytical model for calculating the nonlinear distortion in silicon-based electro-optic Mach–Zehnder modulators," *J. Lightw. Technol.*, vol. 31, no. 23, pp. 3603–3613, Dec. 2013, doi: 10.1109/JLT.2013.2286838.

[15] Y. Zhou *et al.*, "Linearity characterization of a dual–parallel silicon Mach–Zehnder modulator," *IEEE Photon. J.*, vol. 8, no. 6, pp. 1–8, Dec. 2016, doi: 10.1109/JPHOT.2016.2616488.

[16] A. Khilo, C. M. Sorace, and F. X. Kärtner, "Broadband linearized silicon modulator," *Opt. Exp.*, vol. 19, pp. 4485–4500, 2011.

[17] Q. Zhang *et al.*, "Linearity comparison of silicon carrier-depletion-based single, dual-parallel, and dual-series Mach–Zehnder modulators," *J. Lightw. Technol.*, vol. 36, no. 16, pp. 3318–3331, Aug. 2018, doi: 10.1109/JLT.2018.2839603.

[18] J. Sun, R. Kumar, M. Sakib, J. B. Driscoll, H. Jayatilleka, and H. Rong, "A 128 Gb/s PAM4 silicon microring modulator with integrated thermo-optic resonance tuning," *J. Lightw. Technol.*, vol. 37, no. 1, pp. 110–115, Jan. 2019.

[19] B.-M. Yu, J.-M. Lee, C. Mai, S. Lischke, L. Zimmermann, and W.-Y. Choi, "Single-chip Si optical single-sideband modulator," *Photon. Res.*, vol. 6, pp. 6–11, 2018.
[20] A. Ayazi, T. Baehr-Jones, Y. Liu, A. E.-J. Lim, and M. Hochberg, "Linearity of silicon ring modulators for analog optical links," *Opt. Exp.*, vol. 20, pp. 13115–13122 2012.
[21] M. Song, L. Zhang, R. G. Beausoleil, and A. E. Willner, "Nonlinear distortion in a silicon microring-based electro-optic modulator for analog optical links," *IEEE J. Sel. Topics Quantum Electron.*, vol. 16, no. 1, pp. 185–191, Jan./Feb. 2010, doi: 10.1109/JSTQE.2009.2030154.
[22] A. Jain, *et al.*, "A high spur-free dynamic range silicon DC kerr ring modulator for RF applications," *J. Lightw. Technol.*, vol. 37, no. 13 pp. 3261–3272 Jul. 2019.
[23] Q. Zhang, H. Yu, Z. Fu, P. Xia, X. Wang, "Improving the linearity of silicon ring modulators by manipulating the quality factor and operation wavelength," in *Proc. SPIE 11279, Terahertz, RF, Millimeter, Submillimeter-Wave Technol. Appl.*, Mar. 2, 2020, Art. no. 112791T, https://doi.org/10.1117/12.2542242.
[24] M. J. Shin, Y. Ban, B. Yu, J. Rhim, L. Zimmermann, and W. Choi, "Parametric characterization of self-heating in depletion-type Si microring modulators," *IEEE J. Sel. Topics Quantum Electron.*, vol. 22, no. 6, pp. 116–122, Nov./Dec. 2016, doi: 10.1109/JSTQE.2016.2560149.
[25] M.-J. Shin, B.-M. Yu, L. Zimmermann, and W.-Y. Choi, "Parametric characterization of self-heating in Si micro-ring modulators," in *Proc. IEEE 13th Int. Conf. Group IV Photon. (GFP)*, Shanghai, China, 2016, pp. 66–67, doi: 10.1109/GROUP4.2016.7739112.
[26] M. Shin *et al.*, "A linear equivalent circuit model for depletion-type silicon microring modulators," *IEEE Trans. Electron Devices*, vol. 64, no. 3, pp. 1140–1145, Mar. 2017, doi: 10.1109/TED.2017.2648861.
[27] J. Rhim, Y. Ban, B.-M. Yu, J.-M. Lee, and W.-Y. Choi, "Verilog-A behavioral model for resonance-modulated silicon micro-ring modulator," *Opt. Exp.*, vol. 23, pp. 8762–8772 2015.
[28] B. J. Frey, D. B. Leviton, T. J. Madison, "Temperature-dependent refractive index of silicon and germanium," in *Proc. Optomechan. Technol. Astron.*, Jul. 6, 2006, vol. 6273, Art. no. 62732J, [Online]. Available: https://doi.org/10.1117/12.672850.
[29] H. K. Tsang and Y. Liu, "Nonlinear optical properties of silicon waveguides," *Semicond. Sci. Technol.*, vol. 23, no. 6, 2008, Art. no. 064007.
[30] J. Leuthold, C. Koos, and W. Freude, "Nonlinear silicon photonics," *Nature Photon.*, vol. 4, pp. 535–544, 2010.
[31] A. C. Turner-Foster *et al.*,"Ultrashort free-carrier lifetime in low-loss silicon nanowaveguides," *Opt. Exp.*, vol. 18, pp. 3582–3591 2010.
[32] W. B. Bridges and J. H. Schaffner, "Distortion in linearized electrooptic modulators," *IEEE Trans. Microw. Theory Techn.*, vol. 43, no. 9, pp. 2184–2197, Sep. 1995, doi: 10.1109/22.414563.
[33] C. H. Cox, E. I. Ackerman, and G. E. Betts, "Relationship between gain and noise figure of an optical analog link," in *Proc. IEEE MTT-S Int. Microw. Symp. Dig.*, San Francisco, CA, USA, 1996, vol. 3, pp. 1551–1554, doi: 10.1109/MWSYM.1996.512232.

Young kwan Jo (Graduate Student Member, IEEE) received the B.S. degree in 2017 in electrical and electronic engineering from Yonsei University, Seoul, South Korea, where he is currently working toward the Ph.D. degree. His research interests include design, modeling, and optimization of Si photonic optical devices for high-speed optical interconnect.

Christian Mai received the master's degree in physics from Technical University Cottbus, Cottbus, Germany, in 2012. He is currently a Researcher with Technology Department, IHP—Leibniz Institute für innovative Mikroelektronik, Frankfurt, Germany. His research is focuses on the monolithic integration of silicon photonics components in the established 0.25-μm BiCMOS technology of the IHP for the development of an electronic photonic integrated circuits technology.

Stefan Lischke (Student Member, IEEE) received the B.Sc. and M.Sc. degrees in physics with specialization in semiconductor technology from Technical University Brandenburg, Cottbus, in 2005 and 2007, respectively, and the Ph.D. degree in physics from Technical University Berlin, Berlin, Germany, in 2017. He is currently a Researcher with the Silicon Photonics Group, Technology Department of IHP—Leibniz Institute für innovative Mikroelektronik, Frankfurt, Germany. His current work is focused on Germanium photo detectors and the integration of photonic devices into IHP's photonic BiCMOS technology. He was the recipient of the several best paper awards.

Lars Zimmermann (Senior Member, IEEE) was born in Germany. He received a higher education (undergraduate) from Friedrich-Schiller University, Jena, Germany, Brunel University London, London, U.K., and TU Delft, Delft, The Netherlands, and the Ph.D. degree from IMEC, Leuven, Belgium, in 2003. He moved to Belgium for his postgraduate studies at Katholieke Universiteit Leuven. In Leuven, he was affiliated with IMEC, where he worked for five years. His scientific work at IMEC dealt with the development of extended short-wave infrared detector arrays and sensor assembly processes. In 2004, he moved to TU Berlin. In Berlin, he worked for five years on silicon-based optical motherboard technology, realizing early hybrid assemblies of silicon waveguides with lasers, semiconductor optical amplifiers, and detectors. In 2008, he moved to IHP, the Leibniz Institute für innovative Mikroelektronik. At IHP, he directs the silicon photonics activities. In 2018, he re-joined TU Berlin, where he is currently a Professor in the field of silicon photonics. He is also a Team Leader Silicon photonics at IHP, coordinating the cooperation with TU Berlin in the field of Silicon photonics within the frame of the Joint Lab Silicon Photonics. His current work is focusing on high-performance photonic-electronic integration for optical communications and for nonlinear optical signal processing.

Woo-Young Choi (Member, IEEE) received the B.S., M.S., and Ph.D. degrees in electrical engineering and computer science from the Massachusetts Institute of Technology, Cambridge, MA, USA, in 1986, 1988, and 1994, respectively. His doctoral dissertation concerned the investigation of molecular-beam epitaxygrown InGaAlAs laser diodes for fiber-optic applications. From 1994 to 1995, he was a Postdoctoral Research Fellow with NTT Opto-Electronics Laboratories, where he worked on femtosecond all-optical switching devices based on low-temperature grown InGaAlAs quantum wells. In 1995, he joined the Department of Electrical and Electronic Engineering, Yonsei University, Seoul, South Korea, where he is currently a Professor. His research interests include high-speed circuits and systems that include high-speed optoelectronics, high-speed electronic circuits, and silicon photonics.